Journal of Theoretical Biology 314 (2012) 23–33

Contents lists available at SciVerse ScienceDirect

Journal of Theoretical Biology

journal homepage: www.elsevier.com/locate/yjtbi

Mathematical model of intimal thickening in atherosclerosis: Vessel stenosis as a free boundary problem

Pak-Wing Fok *

Department of Mathematical Sciences, University of Delaware, Newark, DE 19716, United States

HIGHLIGHTS

- We model atherosclerotic intimal thickening as a free boundary problem.
- We perform a bifurcation analysis of an associated ordinary differential equation.
- We compare our results to experimental data from Stadius et al. (1992).

ARTICLE INFO

Article history:
Received 26 May 2012
Received in revised form
25 July 2012
Accepted 31 July 2012
Available online 10 August 2012

Keywords:
Eroded plaque
Platelet-derived growth factor
Chemotaxis
Inflammation

ABSTRACT

Atherosclerosis is an inflammatory disease of the artery characterized by an expansion of the intimal region. Intimal thickening is usually attributed to the migration of smooth muscle cells (SMCs) from the surrounding media and proliferation of SMCs already present in the intima. Intimal expansion can give rise to dangerous events such as stenosis (leading to stroke) or plaque rupture (leading to myocardial infarction).

In this paper we propose and study a mathematical model of intimal thickening, posed as a free boundary problem. Intimal thickening is driven by damage to the endothelium, resulting in the release of cytokines and migration of SMCs. By coupling a boundary value problem for cytokine concentration to an evolution law for the intimal area, we reduce the problem to a single nonlinear differential equation for the luminal radius. We analyze the steady states, perform a bifurcation analysis and compare model solutions to data from rabbits whose iliac arteries are subject to a balloon pullback injury. In order to obtain a favorable fit, we find that migrating SMCs must enter the intima very slowly compared to cells in dermal wounds. This cell behavior is indicative of a weak inflammatory response which is consistent with atherosclerosis being a chronic inflammatory disease.

1. Introduction

Atherosclerosis is an inflammatory disease of medium-to-large sized arteries that is often the underlying cause for many adverse cardiovascular conditions. According to the latest statistics (Roger et al., 2012), more than 2200 Americans died of cardiovascular disease every day in 2008, and coronary heart disease was responsible for about 1 out of every 6 deaths in the United States. The prevention and treatment of atherosclerosis, and heart disease in general, is one of the most important problems in medicine today.

The vessel wall undergoes fundamental mechanical and biological changes as atherosclerosis progresses. An artery wall consists of three main layers: an innermost *intima* is surrounded by the *media* that is in turn surrounded by the *adventitia*. The intima in normal, healthy arteries consists of a thin layer of connective tissue and the endothelium, a single layer of cells that lines the inner surface of the entire vasculature. The intima in healthy arteries is typically only a few cell diameters thick. However, one of the defining characteristics of atherosclerosis is an enlarged intima; its growth is mainly attributed to smooth muscle cell (SMC) migration and proliferation. Migration and proliferation occur because cytokines are released into the vessel wall when the endothelium is injured. The nature and source of such an injury is still an active area of research, but could include hemodynamical (Vincent et al., 2011), mechanical (Thubrikar, 2007) or biochemical (Keaney, 2000) insult. These growth factors stimulate SMCs to enter the intima from the surrounding media and may also promote mitosis in cells already present in the intima.

Intimal expansion can result in either positive or negative remodeling. In positive remodeling, the internal elastic lamina

* Tel.: +1 302 831 2266.
E-mail address: pakwing@udel.edu

0022-5193/$ - see front matter © 2012 Elsevier Ltd. All rights reserved.
http://dx.doi.org/10.1016/j.jtbi.2012.07.029

(IEL) surrounding the intima expands outwards while the luminal area remains largely unchanged. This kind of remodeling is characteristic of plaques such as Thin-Capped Fibroatheromas (TCFAs). Such plaques are highly inflamed and characterized by a thin cap, necrotic core and a large number of foam cells. Because the luminal area is unchanged, these plaques are hard to detect. They are largely asymptomatic until they rupture; when this occurs, myocardial infarction usually ensues (Davies, 1992).

In negative remodeling, it is the luminal area that reduces causing a constriction of the blood vessel ("stenosis"). Blood clots may advect from upstream of the stenosis, become lodged in the constriction and cause strokes. Negative remodeling is a feature of so-called "eroded plaque" (Kolodgie et al., 2002). Such plaques differ from TCFAs in at least three different ways. First the endothelium is often absent in eroded plaques. Second, they are less inflamed and contain fewer macrophages. Finally thrombi can develop without plaque rupture. It is thought that the thrombus gradually develops over time as a result of a chronic wound healing response: the denuded lumen is repeatedly eroded away and healed resulting in platelet aggregation and a growing thrombus.

While an *in silico* model of atherosclerosis that incorporates the action of cells, cytokines, hemodynamics and mechanics is not yet available, it is becoming more common to analyze the mechanisms behind plaque formation through mathematical models. Typically, the models either take the form of ODEs (ordinary differential equations) or PDEs (partial differential equations). In ODE models such as (Bulelzai and Dubbeldam, 2012; Ougrinovskaia et al., 2010), the authors study the interaction of macrophages and foam cells inside a plaque; monocytes transform into macrophages after they adhere to the vessel wall. Macrophages then transform into foam cells upon ingesting oxidized low density lipoprotein. On the other hand, in PDE models such as Fok (2011) and Ibragimov et al. (2005), the authors consider cell densities in arterial cross-sections; the goal is for the equations to reproduce the main features of plaque such as its necrotic or lipid core. In Calvez et al. (2010), a more complex model is proposed that couples hemodynamics to the transport of different cell populations and chemical species through the endothelium.

In this paper, we present a model of intimal thickening represented as a free boundary problem, which makes it quite different to the forementioned papers. The radius of the lumen decreases due to the migration and proliferation of SMCs in the intima and our model describes the time evolution of this radius. We reduce the problem to a single ordinary differential equation and analyze its behavior for short and long times. We also analyze its steady states, perform a bifurcation analysis and finally compare our results to data from the arteries of New Zealand white rabbits.

The outline of this paper is as follows: in Section 2, we present the governing equations for our problem along with a non-dimensionalization. In Section 3 we discuss our results and explain the biological insight that our model generates. We end with a conclusion in Section 4.

2. Governing equations

Here we set up the problem of arterial stenosis as a free boundary problem. We consider the problem with concentric geometry, described with polar coordinates (see Fig. 1(a)). With the lumen–intimal interface as a free boundary, described through the lumen radius, our goal is to derive an evolution equation for $\hat{R}_1(\hat{t})$ (where $\hat{t}$ is time) in terms of cell proliferation, death and migration that can occur within the intima.

The migration of SMCs into the intima is regulated by growth factors and cytokines that are released when the endothelium is injured. In fact, experiments on rat carotid artery (Clowes, 1983) show that intimal thickening occurs only when endothelial cells are absent from the inner surface. When the endothelial cells regenerate, intimal thickening stops. The most potent of these cytokines is PDGF (Platelet Derived Growth Factor) which is the focus of our modeling effort.

The distribution of PDGF can be described by the quasi-steady state diffusion–degradation equation

$$D_1\nabla^2\hat{P}_1 - k\hat{P}_1 = 0 \quad \text{on } \hat{R}_1(\hat{t}) < \hat{r} < \hat{R}_2, \tag{1}$$

$$D_2\nabla^2\hat{P}_2 - k\hat{P}_2 = 0 \quad \text{on } \hat{r} > \hat{R}_2, \tag{2}$$

where $\hat{P}_1$ is the concentration of growth factor within the intima and $\hat{P}_2$ is the concentration within the media—see Fig. 1(a). The boundary, interface and far-field conditions are

$$\hat{P}_1 = \hat{f}(\hat{\theta}) \quad \text{on } \hat{r} = \hat{R}_1(\hat{t}), \tag{3}$$

$$\hat{P}_1 = \hat{P}_2 \quad \text{on } \hat{r} = \hat{R}_2, \tag{4}$$

$$D_1\frac{\partial\hat{P}_1}{\partial\hat{r}} = D_2\frac{\partial\hat{P}_2}{\partial\hat{r}} \quad \text{on } \hat{r} = \hat{R}_2, \tag{5}$$

$$\hat{P}_2 \to 0 \quad \text{as } \hat{r} \to \infty. \tag{6}$$

We ignore any convection of PDGF due to radial transmural flow because our goal is to derive the simplest model that includes the effect of SMC migration induced by cytokine gradients.

This quasi-steady state approximation is justified if the time taken for PDGF to reach its steady state is much shorter than the time scale of stenosis. In (1) and (2), D_1 and D_2 are the diffusion constants for PDGF in the intima and media respectively and k is its degradation rate. In (4) and (5), we have imposed continuity of PDGF and its flux across the IEL. The function $\hat{f}(\hat{\theta})$ is a compactly supported function, taking only non-zero values for $|\hat{\theta}| < \hat{\theta}_0/2$ (see Fig. 1(a)). Biologically, $\hat{f}$ can be thought of as representing an injury to the endothelium.

What is the source of endothelial damage? Endothelial injury could arise because of rapidly changing hemodynamical shear stress on the endothelium: the mitotic rate of endothelial cells appears to be higher near bifurcations of the artery (Thubrikar, 2007) where the flow may locally recirculate and be far from laminar. Because of the injury, platelets adhere to the endothelium, releasing cytokines such as PDGF. These platelets form a solid thrombus—see Chapter 4 in Virmani et al. (2007) and Fig. 1(b) and (c). In principle, the growth of this thrombus depends on the local hemodynamics and the biochemistry of clotting (Guy et al., 2007). However, in this paper, we do not account for this thrombus explicitly. Instead, we only model its release of PDGF. Because a thrombus is essentially a blood clot composed of platelets and fibrin, it is resistant to deformation and we expect that the footprint of the thrombus may stay approximately constant in time. When the lumen constricts, the angle of injury $\hat{\theta}_0(\hat{t})$ increases as endothelial cells are strained and damaged.

Let $\hat{\theta}_0(0)$ be the initial angle of injury, so that the initial *area* of injury (per unit length of artery) is $\hat{R}_1(0)\hat{\theta}_0(0)$. For subsequent times, we assume that this area remains constant so $\hat{R}_1(\hat{t})\hat{\theta}_0(\hat{t}) = \hat{R}_1(0)\hat{\theta}_0(0)$ for $\hat{t} > 0$. This damaged area acts as the primary source of PDGF since platelets release PDGF when they adhere to the site of injury. We take

$$\hat{f}(\hat{\theta};\hat{R}_1(\hat{t})) = \begin{cases} P_0, & |\hat{\theta}| < \min\left(\dfrac{\hat{\theta}_0(t)}{2},\pi\right), \quad \hat{\theta}_0(\hat{t}) = \dfrac{\hat{R}_2\hat{\theta}_0(0)}{\hat{R}_1(\hat{t})} \\ 0 & \text{otherwise,} \end{cases} \tag{7}$$

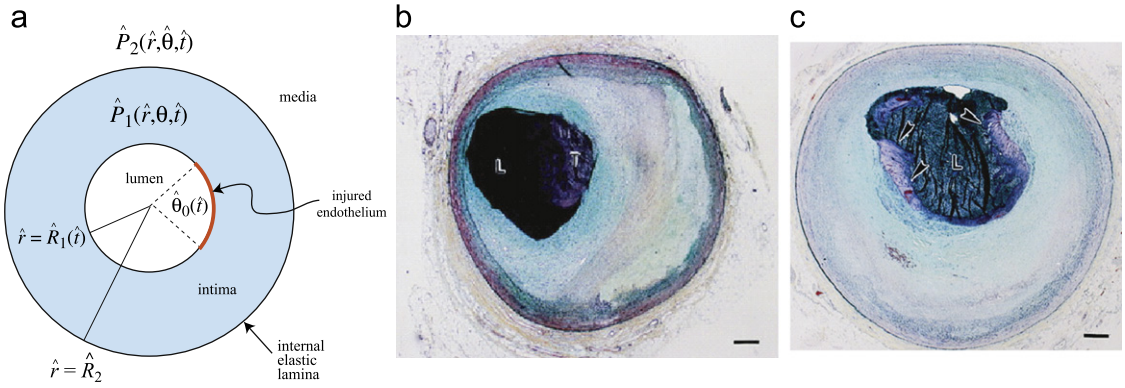

Fig. 1. (a) Schematic of a thickened intima, represented here as the region between two concentric circles with radii $\hat{R}_1$ and $\hat{R}_2$. $\hat{P}_1$ and $\hat{P}_2$ are distributions of PDGF (Platelet Derived Growth Factor) in the intima and media respectively. (b) and (c) Stained cross-sections of eroded plaques taken from Farb et al. (1996). Scale bars represent 0.375 mm. In (b) a thrombus labeled "T" can be seen as a result of endothelial injury and in (c) the thrombi are indicated with arrowheads.

where P_0 is a typical PDGF concentration at the injury site. The arclength of injured endothelium, $\hat{R}_1(\hat{t})\hat{\theta}_0(\hat{t})$, remains constant in time until the entire endothelium is inflamed, in which case $\hat{f}(\hat{\theta})=P_0$ for $0\le\hat{\theta}\le 2\pi$.

An injury to the endothelium encourages adhesion of platelets and locally increases concentrations of plasmin which is proteolytic. By degrading extra-cellular matrix (ECM) plasmin frees SMCs, allowing them to respond to chemoattractants such as PDGF (Jackson et al., 1993). In fact, experiments on thrombocytopenic rats (which have $<1\%$ of the platelet count of normal animals) show that they have fewer intimal SMCs than normal rats (Jackson et al., 1993). In our model, we assume that SMCs chemotax from the media up concentration gradients in released PDGF and proliferate. Both effects can result in an expansion of the intima.

Applying conservation of mass to the intimal region $\hat{\Omega}=\{(\hat{r},\hat{\theta}):\hat{R}_1<\hat{r}<\hat{R}_2\}$, we have

$$\frac{\mathrm{d}}{\mathrm{d}\hat{t}}\int\int_{\hat{\Omega}}\hat{\rho}(\hat{r},\hat{t})\,\mathrm{d}\hat{\Omega}+\oint_{\partial\hat{\Omega}}\hat{\mathbf{j}}\cdot\mathbf{n}\,\mathrm{d}\hat{s}=\int\int_{\hat{\Omega}}[\Pi_0-\hat{\rho}(\hat{r},\hat{t})\Pi_1]\,\mathrm{d}\hat{\Omega},\tag{8}$$

where $\hat{\rho}$ is the density of SMCs, $\hat{\mathbf{j}}$ is the flux of SMCs on $\partial\hat{\Omega}$, $\mathbf{n}$ is the unit outward normal on $\partial\hat{\Omega}$, Π_0 is the proliferation rate per unit area of intima and Π_1 is the death rate of smooth muscle cells which we assume to be constant with respect to space, time and PDGF concentration. Assuming no SMC fluxes on $\hat{r}=\hat{R}_1$, a constant intimal SMC density $\hat{\rho}=\rho_0$ and a PDGF-dependent proliferation rate, $\Pi_0=\Pi_0(\hat{P}_1)$, we obtain an evolution law for the intimal area $\hat{A}(\hat{t})$ in terms of SMC migration from the media and proliferation

$$\rho_0\frac{\mathrm{d}\hat{A}}{\mathrm{d}\hat{t}}=-\oint_{\hat{r}=\hat{R}_2}\hat{\mathbf{j}}\cdot\mathbf{n}\,\mathrm{d}s+\int\int_{\hat{\Omega}}[\Pi_0(\hat{P}_1)-\rho_0\Pi_1]\,\mathrm{d}\hat{\Omega}.\tag{9}$$

In our model the focus is on the biochemical effects of PDGF-induced intimal expansion. The migration of cells into the intima and their proliferation will also induce mechanical stresses in the intima which are not included in our model, but these effects have been treated by other researchers, for example see Amar et al. (2011) and Goriely and Vandiver (2010).

Chemotaxis by PDGF has been quite well characterized through a series of joint experimental and modeling approaches (Haugh, 2006; Park et al., 2003; Schneider and Haugh, 2005). Here we briefly describe a feasible mechanism in order to present a simple model for PDGF-induced chemotaxis. For dermal fibroblast wound healing assays, PDGF binds to receptors on the fibroblast cell surface which then activate by dimerizing with each other and autophosphorylating. In this activated state the receptors can bind with cytosolic enzymes such as PI (phosphoinositide) 3-kinase which releases a family of secondary messengers 3′-PI. Intracellular gradients of 3′-PI modulate the cytoskeleton resulting in cell motion.

A derivation of the familiar Keller–Segel chemotaxis law in terms of some of the microscopic processes described above is given in Keener and Sneyd (2009). Let $\hat{P}$ be the concentration of chemoattractant. For small gradients in $\hat{P}$, the cell speed is derived as $\mathbf{v}=v_0\chi_0N_b'(\hat{P})\nabla\hat{P}$ where v_0 is the maximum cell speed, χ_0 is the *chemotactic sensitivity* and $N_b(\hat{P})$ is the number of activated receptors as a function of chemoattractant. Hill functions are usually prescribed for $N_b(\hat{P})$. If we assume that the binding of PDGF to its receptor is rate limiting, then we have a Hill coefficient equal to unity and $N_b(\hat{P})=N_T\hat{P}/(K_d+\hat{P})$ where N_T is the total number of PDGF receptors on the cell surface and K_d is the dissociation constant of PDGF/PDGF-receptor binding. Furthermore, if $\hat{P}\ll K_d$, then $N_b'(\hat{P})\approx N_T/K_d$.

When $D_1=D_2$, $\nabla\hat{P}_1=\nabla\hat{P}_2=\nabla\hat{P}$ at $\hat{r}=\hat{R}_2$ and the SMC flux is

$$\hat{\mathbf{j}}|_{\hat{r}=\hat{R}_2}=\rho_s\mathbf{v}=\frac{v_0\chi_0N_T}{K_d}\rho_s\nabla\hat{P},\tag{10}$$

where ρ_s is the pore density of the IEL. If there was no barrier at all to SMC migration, then the mass flux of SMCs (per unit area of IEL) into the intima would be the product of the medial SMC density and SMC migration velocity. However, the fibrous IEL physically separates the intima from the media; see Fig. 1(a). This IEL is *fenestrated* so that SMCs and other low molecular weight substances can pass through pores of the IEL that typically range from 0.4–4 μm in diameter. Hence, the mass flux of SMCs is modulated by the pore density.

When $D_1\neq D_2$ in (5), $\nabla\hat{P}_1|_{\hat{R}_2}\neq\nabla\hat{P}_2|_{\hat{R}_2}$. In practice, we expect that gradients in the PDGF concentration will change rapidly – but smoothly – near the media–intima interface so SMCs will respond to some weighted average of $\nabla\hat{P}_1|_{\hat{R}_2}$ and $\nabla\hat{P}_2|_{\hat{R}_2}$, the gradients inside and outside of the IEL. In this study we take

$$\hat{\mathbf{j}}|_{\hat{r}=\hat{R}_2}=\frac{\rho_s\chi}{2}(\nabla\hat{P}_1|_{\hat{R}_2}+\nabla\hat{P}_2|_{\hat{R}_2}),\quad\chi=\frac{v_0\chi_0N_T}{K_d}.\tag{11}$$

Finally, since the concentration of PDGF is low in a chronic response, we use a linear approximation for the proliferation rate. We assume that SMCs reproduce most quickly when concentrations of PDGF are maximal, close to the site of injury. We take

$$\Pi_0(\hat{P})=\frac{Q_0\hat{P}}{P_0},\tag{12}$$

where Q_0 is the maximum proliferation rate.

Table 1 summarizes the dimensional constants of our problem. Naturally, several parameters span a range of values. For example, the SMC proliferation rate Q_0, calculated from Fig. 4 in Tsai et al. (1994) is highly dependent on the culture conditions. More details

Table 1
Parameter values for Eqs. (1)–(12). IEL=Internal Elastic Lamina, PDGF=Platelet Derived Growth Factor, SMC=Smooth Muscle Cell.

Parameter	Description	Value/Range	Ref
$\hat{R}_2$	IEL radius	1 mm	–
k	PDGF degradation rate	0.1 h^{-1}	Haugh (2006)
D_1	PDGF diffusion constant in intima	0.01 mm^2/h	Haugh (2006)
D_2	PDGF diffusion constant in media	0.01 mm^2/h	Haugh (2006)
P_0	Maximum PDGF concentration	0.1 nM	Haugh (2006)
ρ_0	SMC density in intima	800 mm^{-2}	Virmani et al. (2007, p. 64)
ρ_s	Pore density in IEL	1000–50,000 mm^{-2}	Tada and Tarbell (2000)
Q_0	SMC proliferation rate	0.3–10 $mm^{-2}\,h^{-1}$	Tsai et al. (1994)
Π_1	SMC death rate	$6\times10^{-3}\,h^{-1}$	Bennett et al. (1995)
v_0	Maximum SMC migration speed	0.1 mm/h	Haugh (2006)
χ_0	Chemotactic sensitivity	2×10^{-5} cm/receptor	Keener and Sneyd (2009)
N_T	# PDGF receptors on SMC surface	10^5 receptors	Park et al. (2003)
K_d	Dissoc. const. of PDGF from receptors	1.47 nM	Park et al. (2003)

on how the dimensional constants are estimated can be found in Appendix B.

2.1. Non-dimensionalization

We now introduce the dimensionless quantities

$$r=\frac{\hat{r}}{\hat{R}_2},\quad \theta=\hat{\theta},\quad P_{1,2}=\frac{\hat{P}_{1,2}}{P_0},\quad t=\Pi_1\hat{t},\quad R=\frac{\hat{R}_1}{\hat{R}_2},\quad A=\frac{\hat{A}}{\hat{R}_2^2}, \tag{13}$$

so that the dimensional outer radius $\hat{R}_2$ is mapped to a dimensionless unit radius. Our dimensionless diffusion–degradation equations are

$$\frac{\partial^2P_1}{\partial r^2}+\frac{1}{r}\frac{\partial P_1}{\partial r}+\frac{1}{r^2}\frac{\partial^2P_1}{\partial\theta^2}-\lambda_1^2P_1(r)=0,\quad R(t)\le r<1, \tag{14}$$

$$\frac{\partial^2P_2}{\partial r^2}+\frac{1}{r}\frac{\partial P_2}{\partial r}+\frac{1}{r^2}\frac{\partial^2P_2}{\partial\theta^2}-\lambda_2^2P_2(r)=0,\quad r\ge1, \tag{15}$$

where $\lambda_{1,2}=\sqrt{k/D_{1,2}}\hat{R}_2$. The boundary conditions become

$$P_1(r,\theta)=f(\theta;R)\quad\text{on } r=R(t), \tag{16}$$

$$P_1(r,\theta)-P_2(r,\theta)=0\quad\text{on } r=1, \tag{17}$$

$$\lambda_2^2\frac{\partial P_1(r,\theta)}{\partial r}-\lambda_1^2\frac{\partial P_2(r,\theta)}{\partial r}=0\quad\text{on } r=1, \tag{18}$$

$$P_2(r,\theta)\to0\quad\text{as } r\to\infty, \tag{19}$$

where $f\equiv\hat{f}/P_0$ and the dimensionless evolution equation for the intimal area $A(t)=\pi(1-R^2(t))$ is

$$\frac{dA}{dt}=-\alpha\int_{-\pi}^{\pi}\left[\left.\frac{\partial P_1}{\partial r}\right|_{r=1}+\left.\frac{\partial P_2}{\partial r}\right|_{r=1}\right]d\theta+\beta\int_{-\pi}^{\pi}\int_{R(t)}^{1}P_1(r,\theta)r\,dr\,d\theta-A(t), \tag{20}$$

where $A(0)=0$,

$$\alpha=\frac{\rho_s v_0\chi_0N_TP_0}{2\rho_0\hat{R}_2^2\Pi_1K_d},\quad \beta=\frac{Q_0}{\rho_0\Pi_1}, \tag{21}$$

and

$$f(\theta,R(t))=\begin{cases}1, & |\theta|<\min\left(\dfrac{\theta_0(t)}{2},\pi\right),\quad \theta_0(t)=\theta_0(0)/R(t),\\ 0 & \text{otherwise.}\end{cases} \tag{22}$$

Eq. (20), coupled to the boundary value problem (14)–(19), defines our free boundary problem: Eq. (20) is an ordinary differential equation (ODE) for $A(t)$ where the right hand side depends on the solution to (14)–(19). As $A(t)$ evolves, so does the domain of solution of (14)–(15) and the boundary condition (16) and (22): the quasi-steady distribution of PDGF evolves in time along with the intimal area.

We now reduce the two coupled problems to a single ODE for the radius $R(t)$. This can be done by solving for $P_{1,2}(r,\theta)$ explicitly using separation of variables and directly substituting into (20); details can be found in Appendix A. After some calculation, we find

$$\begin{aligned}\dot{R}&=F(R;\alpha,\beta,\theta_0(0),\lambda_1,\lambda_2),\\ &:=-\frac{\alpha\sigma[R;\theta_0(0)]C_1(\lambda_1,\lambda_2)}{R\Delta_0(R)}+\frac{1}{2}\left(\frac{1-R^2}{R}\right)\\ &\quad-\frac{\beta\sigma[R;\theta_0(0)]}{R\Delta_0(R)\lambda_1}\{C_2(\lambda_1,\lambda_2)[RK_1(\lambda_1R)-K_1(\lambda_1)]-C_3(\lambda_1,\lambda_2)[RI_1(\lambda_1R)-I_1(\lambda_1)]\},\end{aligned} \tag{23}$$

subject to the initial condition $R(0)=1$, where

$$\sigma[R;\theta_0(0)]=\min\left[\frac{\theta_0(0)}{2\pi R},1\right], \tag{24}$$

$$\begin{aligned}\Delta_0(R)&=\lambda_1K_1(\lambda_2)[I_0(\lambda_1)K_0(\lambda_1R)-K_0(\lambda_1)I_0(\lambda_1R)]\\ &\quad+\lambda_2K_0(\lambda_2)[I_1(\lambda_1)K_0(\lambda_1R)+K_1(\lambda_1)I_0(\lambda_1R)],\end{aligned} \tag{25}$$

and $I_1(\cdot)$ and $K_1(\cdot)$ are modified Bessel functions of the first and second kind respectively. Note that $\Delta_0(R)>0$ if $0<R<1$ since $I_0(\lambda_1)>I_0(\lambda_1r)$ and $K_0(\lambda_1r)>K_0(\lambda_1)$ when $0\le R<r<1$.

The constants C_1, C_2 and C_3 are defined in terms of λ_1 and λ_2

$$C_1(\lambda_1,\lambda_2)=(\lambda_1^2+\lambda_2^2)[K_1(\lambda_1)K_1(\lambda_2)I_0(\lambda_1)+K_0(\lambda_1)K_1(\lambda_2)I_1(\lambda_1)], \tag{26}$$

$$C_2(\lambda_1,\lambda_2)=\lambda_1K_1(\lambda_2)I_0(\lambda_1)+\lambda_2K_0(\lambda_2)I_1(\lambda_1), \tag{27}$$

$$C_3(\lambda_1,\lambda_2)=-\lambda_1K_1(\lambda_2)K_0(\lambda_1)+\lambda_2K_0(\lambda_2)K_1(\lambda_1). \tag{28}$$

In (23), F is the sum of three terms. The first term, proportional to α, is always negative and represents stenosis due to cell migration. The second term is always positive and represents a lumen expansion due to cell death. The final term, proportional to β, represents intimal expansion due to cell proliferation. This term is always negative because

$$\begin{aligned}&C_2[RK_1(\lambda_1R)-K_1(\lambda_1)]-C_3[RI_1(\lambda_1R)-I_1(\lambda_1)]\\ &\quad=\lambda_1\int_R^1\Delta_0(r)r\,dr,>0.\end{aligned} \tag{29}$$

The solution of the ODE (23) is therefore determined by 5 dimensionless constants: the chemotactic parameter α, the proliferation parameter β, the initial angle of injury $\theta_0(0)$ and the two parameters of the steady-state diffusion–degradation equation λ_1 and λ_2. The numerical value of these parameters can be derived from Table 1; in Section 3.2 we will compare the calculated values to values derived from experimental data.

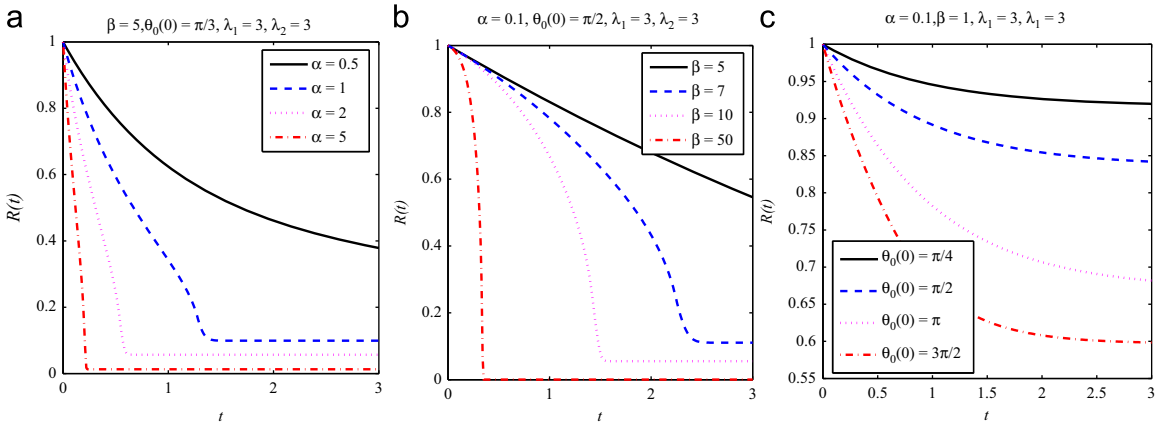

Fig. 2. Vessel stenosis over time as predicted by (23) when (a) migration parameter α, (b) proliferation parameter β (c) initial angle of injury $\theta_0(0)$ varies.

3. Results and discussion

In Fig. 2 we plot solutions of the ODE (23) for different values of α, β and $\theta_0(0)$. In (a) we see that as the migration parameter α is increased, the rate of stenosis increases and the steady state value for $R(t)$ decreases. A larger value of α implies a larger cell flux into the intima and therefore a faster decrease in $R(t)$. In Fig. 2(b) and (c) a similar effect can be seen as the proliferation parameter β and initial angle of injury $\theta_0(0)$ are increased. We see that when β is large, the radius rapidly drops as SMCs quickly reproduce to enlarge the intimal region. Likewise, when $\theta_0(0)$ is large, more SMCs are recruited from the media since a greater portion of the internal elastic lamina is inflamed (as indicated by the presence of PDGF); this is discussed below. In all three cases, a steady state is reached as migration and proliferation of SMCs are eventually balanced by SMC death.

An important feature of Eq. (23) which is illustrated in Fig. 2 is that solutions exist for all $t \geq 0$. In particular, $R(t) > 0$ for $t \geq 0$. If $\alpha > 0$ and $0 < \theta_0(0) \leq 2\pi$, then

$$F(R=1) = -\frac{\alpha\sigma(1)C_1}{\lambda_2 K_0(\lambda_2)[I_1(\lambda_1)K_0(\lambda_1)+K_1(\lambda_1)I_0(\lambda_1)]} < 0, \tag{30}$$

but

$$F(R) \sim \frac{1}{2R} + \frac{\alpha C_1 + \frac{\beta}{\lambda_1}\left(-C_2K_1(\lambda_1)+C_3I_1(\lambda_1)\right)}{C_2 R \ln(\lambda_1 R/2)} \to +\infty, \tag{31}$$

as $R \to 0^+$. The term $-C_2K_1(\lambda_1)+C_3I_1(\lambda_1) > 0$ using (29) with $R \to 0^+$. Since $F(R)$ is continuous on (0, 1], by the intermediate value theorem, there must exist $0 < R^* < 1$ such that $F(R^*) = 0$, i.e. there is always (at least) one steady state solution in (0, 1). Since $F(R)$ is continuous, this steady state can always be reached given the initial condition $R(0) = 1$ and solutions will exist for all $t \geq 0$.

In Fig. 3, we show a times series of snapshots of the PDGF distribution and the resulting inflammation and vessel stenosis. In these plots, the thick black line represents the IEL that separates the intima from the media (compare with Fig. 1(a)). Although we show the media to have a thickness of 1/2, the outer boundary of the media plays no role in our model (note the far field condition (19) is at $r = +\infty$) and so this choice for the media thickness in Fig. 3 is actually arbitrary. At $t = 0$, the intima has zero area, but as SMCs migrate in, the intima grows, resulting in the formation of "neointima" and forcing the lumen to narrow. In our model, we assumed that there are no SMCs in the intima at $t = 0$ (this is the case with mammals such as rabbits and rats (Newby and Zaltsman, 1999)) and so $A(0) = 0$. Then initially, stenosis must be triggered by cell migration since

$$\dot{R}(t=0) = -\frac{\alpha\theta_0(0)(\lambda_1^2+\lambda_2^2)}{2\pi\lambda_2} \times \frac{K_1(\lambda_1)K_1(\lambda_2)I_0(\lambda_1)+K_0(\lambda_1)K_1(\lambda_2)I_1(\lambda_1)}{K_0(\lambda_1)K_0(\lambda_2)I_1(\lambda_1)+K_0(\lambda_2)K_1(\lambda_1)I_0(\lambda_1)}. \tag{32}$$

Hence the initial decrease in the radius is driven entirely by chemotaxis. Once the intima contains a positive population of SMCs, they can proliferate causing further intimal expansion. At the same time, the angle of injury $\theta_0(t)$ increases as more endothelial cells are damaged during the constriction. When the entire endothelium is injured, the stenosis comes to a halt as $R(t)$ has effectively reached its steady state, as shown in the final three panels of Fig. 3. We now analyze these steady states.

3.1. Bifurcation study

To gain a quantitative understanding of the steady state of Eq. (23), in Fig. 4 we plot $F(R)$ as we change the parameters α, β and $\theta_0(0)$. The function $F(R)$ has a cusp singularity at $R = \bar{R} := \theta_0(0)/2\pi$ since

$$F'(\bar{R}^+) - F'(\bar{R}^-) = \frac{\alpha C_1 + \frac{\beta}{\lambda_1}\{C_2[\bar{R}K_1(\lambda_1\bar{R}) - K_1(\lambda_1)] - C_3[\bar{R}I_1(\lambda_1\bar{R}_1) - I_1(\lambda_1)]\}}{\bar{R}^2\Delta_0(\bar{R})} > 0 \tag{33}$$

using (29) and (26)–(28). It is clear that the jump in the derivative of F at $R = \bar{R}$ increases with the parameters α and β. This analysis is confirmed in Fig. 4 when we plot $F(R)$ for different α, β and $\theta_0(0)$. The implication for solutions $R(t)$ is that when α and/or β is large, the radius rapidly plummets but comes to an abrupt halt near $\bar{R}$ since $F(R)$ is a rapidly decreasing function for $R < \bar{R}$; see Fig. 2(b) for $\beta = 50$, for example. In Fig. 5, we plot the steady states of (23), R^*, as a function of the parameters α, β and $\theta_0(0)$. In Fig. 5(a) for small values of the bifurcation parameter α, we see that there is a single steady state for $R(t)$ but as α is increased past a critical value α_1^*, a saddle node bifurcation occurs[1] and a second steady state appears. This second steady state is semi-stable at $\alpha = \alpha_1^*$ but as α continues to increase, the semi-stable node splits into a stable and unstable node. Unstable nodes are indicated in Fig. 5 with a dashed red line. It is clear that there is a window of values for α for which Eq. (23) has three steady states. As α increases to a second critical value α_2^*, there is a merging and annihilation of the unstable node with the original

[1] A saddle node bifurcation has normal form $\dot{y}(t) = r + y^2$ for parameter r whereas the bifurcation in our system more closely resembles $\dot{y}(t) = r + |y|$, which has a qualitatively similar behavior.

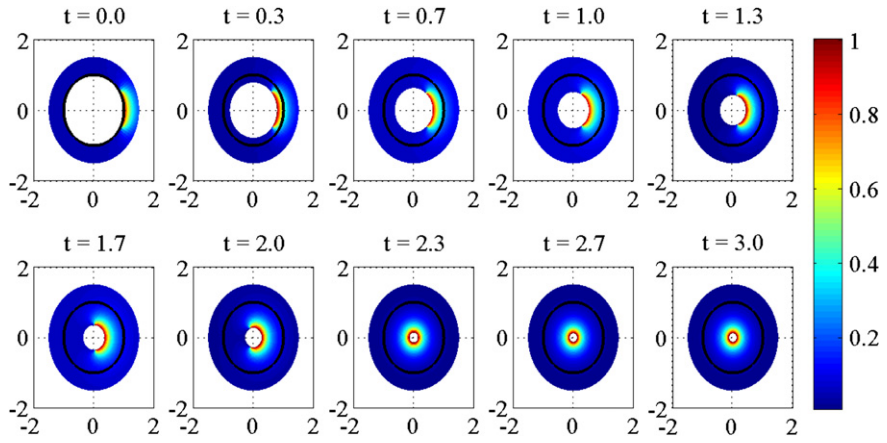

Fig. 3. Time evolution of intimal expansion and subsequent PDGF distribution with $\alpha=1.3$, $\beta=5$, $\theta_0(0)=\pi/4$, $\lambda_1=3$, $\lambda_2=3$.

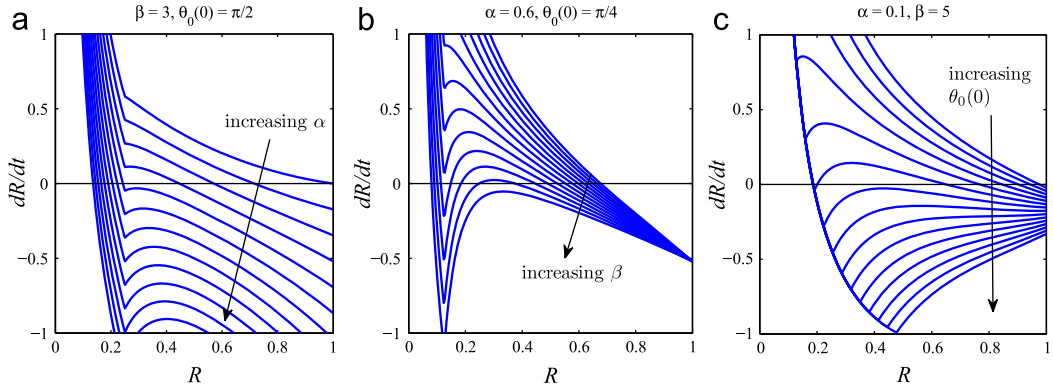

Fig. 4. Right hand side of (23) as (a) α increases from 0 to 1.2 in increments of 0.1, (b) β increases from 1 to 7 in increments of 0.5, (c) $\theta_0(0)$ increases from 0.2 to 3 in increments of 0.2. In all cases, $\lambda_1=\lambda_2=3$.

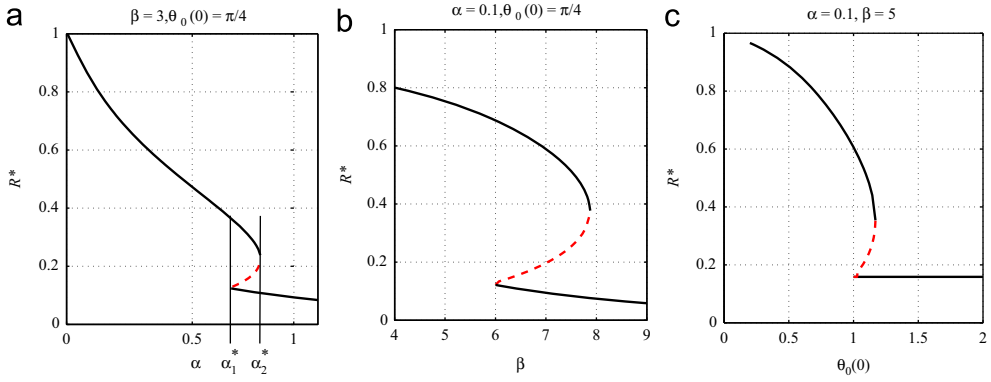

Fig. 5. Bifurcation diagrams showing the steady states R^* for Eq. (23) when $\lambda_1=3$, $\lambda_2=7$ with respect to parameters (a) α, (b) β and (c) $\theta_0(0)$. A solid black line indicates stable fixed points while a dashed red line indicates unstable fixed points. (For interpretation of the references to color in this figure caption, the reader is referred to the web version of this paper.)

stable node leaving just a single, stable, steady state for $\alpha>\alpha_2^*$. The bifurcation behavior in Fig. 5(b) is qualitatively similar. In Fig. 5(c) we see that when $\theta_0(0)\geq 1$, the smallest steady state is independent of $\theta_0(0)$, consistent with Fig. 4(c).

When $\alpha\gg 1$ or $\beta\gg 1$, the steady state $0<R^*\ll 1$. In fact, an asymptotic analysis yields an explicit form for R^*. Since

$$\Delta_0(R)\sim -C_2(\lambda_1,\lambda_2)\left[\ln\frac{\lambda_1 R}{2}+\gamma\right]+O(R^2),\quad R\to 0^+, \tag{34}$$

where $\gamma=0.577215\ldots$ is Euler's constant, we have

$$R^*\sim\frac{2}{\lambda_1}\exp\left(-\frac{2}{C_2}\left[\alpha C_1+\frac{\beta C_3 I_1(\lambda_1)}{\lambda_1}-\frac{\beta C_2 K_1(\lambda_1)}{\lambda_1}\right]\right),\quad R^*\ll 1. \tag{35}$$

Since the term in the square braces is always positive, R^* is exponentially small (but positive) when proliferation and/or migration is dominant in the system. What are the biological implications of these bifurcations? We discuss these below with α

as the bifurcation parameter, but our conclusions also apply to Fig. 5(b) and (c) with β and $\theta_0(0)$ as the bifurcation parameters.

In (a) when $\alpha<\alpha_1^*$ or $\alpha>\alpha_2^*$ there is a single steady state but for $\alpha_1^*<\alpha<\alpha_2^*$, there are three steady states, one of which is unstable. Our model predicts that the lumen of the blood vessel, with initial radius $R(0)=1$, will stenose until it reaches the larger steady state. Because this steady state is stable, providing the background parameters are unchanged, any externally induced increase in $R(t)$ will not change its long time behavior. For patients with arteries severely stenosed with plaque, treatment by balloon angioplasty (mechanical dilation of the blood vessel) results in restenosis in 25% to 50% of patients within six months of the procedure (Shaw et al., 1995). Although our model does not predict the response of the vessel wall under mechanical loads (for this, we refer to Eftaxiopoulos and Atkinson, 2005), it is not surprising from our bifurcation analysis that restenosis occurs: angioplasty does not change the values of α and β and does not directly address the underlying cell dynamics of intimal expansion.

Now suppose that $\alpha_1^*<\alpha<\alpha_2^*$ and the system has reached its larger steady state value. If the migration parameter is further increased outside of the window $[\alpha_1^*,\alpha_2^*]$, the lumen responds with a sudden, catastrophic decrease in R^*. Biologically, such a sudden stenosis may increase the risk of trapped blood clots and stroke.

Ideally we would like to present the bifurcations in Fig. 5 as multi-dimensional plots, showing the steady states R^* as functions of the three parameters α, β and $\theta_0(0)$. Since this is difficult in practice, in Fig. 6, we superimpose several bifurcation plots (with α and β as the bifurcation parameters) for different initial angles of injury $\theta_0(0)$. Depending on the value of $(\alpha,\theta_0(0))$ or $(\beta,\theta_0(0))$, there can be 1, 2 or 3 steady states. Consider Fig. 6(a). For most values of $\theta_0(0)$ in the range $0\le\alpha\le 2$, the system has a single steady state: only for small values of $\theta_0(0)$ do multiple steady states emerge. A similar situation occurs in Fig. 6(b): for a range of β values, there is a single steady state when the initial angle of injury is sufficiently large. When $\theta_0(0)$ is decreased, multiple steady states can arise.

In light of the above arguments, there are two conditions that specify the values of $(\alpha,\beta,\theta_0(0))$ for which there are two real roots in $F(R)$. The first is that

$$F(\bar{R};\alpha,\beta,\theta_0(0))=0 \quad \text{and} \quad F'(\bar{R}^+;\alpha,\beta,\theta_0(0))>0, \tag{36}$$

which states that the cusp of $F(R)$ (where it has a discontinuous derivative) must touch the horizontal axis to give a semi-stable fixed point; we refer back to Fig. 4. At the same time, the right derivative must be positive to ensure a second root for $R>\bar{R}$. For a given $\theta_0(0)$ and β, the solution of (36) defines a functional relation $\alpha=g_-(\beta,\theta_0(0))$. The second condition for the existence of two roots is given by the pair of equations

$$F(R;\alpha,\beta,\theta_0(0))=0, \tag{37}$$

$$F'(R;\alpha,\beta,\theta_0(0))=0, \tag{38}$$

where prime denotes derivative with respect to R. For given β and $\theta_0(0)$, the solution of Eqs. (37) and (38) give a pair α and R. In practice, we rearrange (37) to find $\alpha=g_+(\beta,\theta_0(0);R)$ and then numerically solve $F'(R;g_+(\beta,\theta_0(0);R),\beta,\theta_0(0))=0$ for R, yielding $R=\hat{R}$. The value of α that corresponds to the given $(\beta,\theta_0(0))$ is then defined through $\alpha=g_+(\beta,\theta_0(0);\hat{R})$.

By plotting $\alpha=g_\pm(\beta,\theta_0(0))$, we summarize the multiplicity of steady states in Fig. 7. Regions in $(\alpha,\theta_0(0))$ space with 3 roots are colored in gray; the boundary of these regions where there are two roots is indicated in black. As β increases, the tip of the "horn" region is pulled towards larger $\theta_0(0)$ values, increasing the range of initial angles and migration parameters that may result in a catastrophic stenosis.

3.2. Comparison with experiments

In Fig. 8 we superimpose solutions of our model with data taken from experiments on New Zealand white rabbits (Stadius et al., 1992). In these experiments, a population of rabbits were fed a 2% cholesterol diet. By regularly sacrificing the rabbits, the intimal area of the iliac arteries was monitored over the course of about 40 days. Values of α, β and $\theta_0(0)$ were chosen to best-fit the data in the least-squares sense by minimizing the residual $\mathrm{Res}(\alpha,\beta,\theta_0(0))=\sum_{i=1}^{N}\omega_i[\hat{A}_i-\hat{A}(\hat{t}_i;\alpha,\beta,\theta_0(0))]^2$, where $\hat{A}(\hat{t})=\pi(\hat{R}_2^2-\hat{R}_1^2(\hat{t}))$ is the intimal area, $((\hat{t}_1,\hat{A}_1),\ldots,(\hat{t}_N,\hat{A}_N))$ are the N data points and ω_i are chosen weights (see below for details). For given α, β and $\theta_0(0)$, each evaluation of the residual requires the solution of Eq. (23); because the data is dimensional, we then redimensionalize our solution with $\hat{R}_2=1$ mm and $\Pi_1=6\times10^{-3}$ h^{-1}. MATLAB's constrained optimization routine `fmincon` was used to minimize the residual subject to $0\le\alpha\le0.1$, $0\le\beta\le50$ and $0\le\theta\le2\pi$. Optimal α, β and $\theta_0(0)$ were usually found after about 10 iterations.

When fitting our model curves to the experimental data, there are three possible approaches to take. The first ("uniform") is to

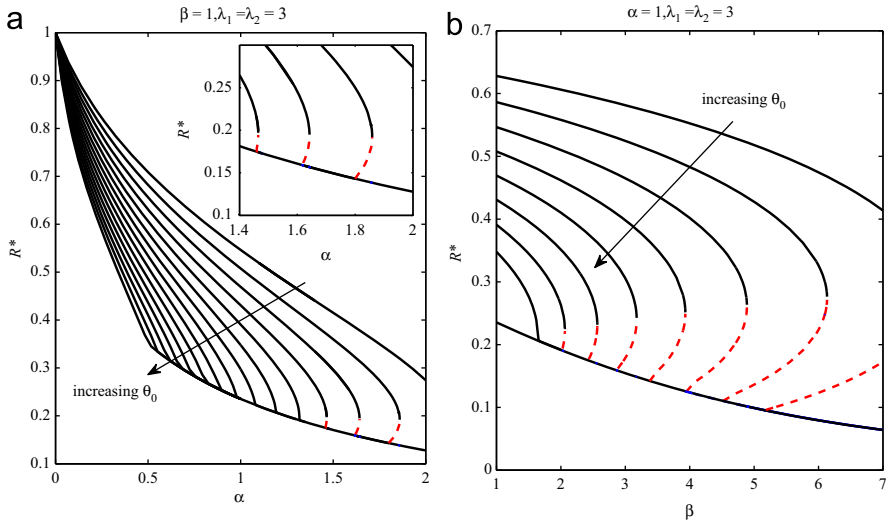

Fig. 6. Bifurcation diagrams as parameters (a) α and (b) β change. These plots are constructed by superimposing the curves in Fig. 5 for different values of $\theta_0(0)$. In (a), θ_0 increases from 0.8 to 2.2 in increments of 0.1. In (b), $\theta_0(0)$ increases from 0.6 to 1.3 in increments of 0.1.

treat all the data points equally: $\omega_i = 1$ for $i = 1, \ldots, N$. However, in the papers of Stadius et al. (1992) and Jackson et al. (1993), the authors were adamant that SMCs only appeared after 3 or 4 days: before this time, there were no SMCs in the intima at all. Since the four earliest time points have much less error than the other points, in the second type of fit ("weighted"), we give the first four points 30× more weight when calculating the residual: $\omega_i = 30$ for $i = 1, \ldots, 4$ and $\omega_i = 1$ for $i = 5, \ldots, N$. The factor of 30 is simply chosen so that there is a visible difference from the uniform fit. Finally, we can ignore the first four time points ("delayed"): $\omega_i = 0$ for $i = 1, \ldots, 4$ and $\omega_i = 1$ for $i = 5, \ldots, N$.

The justification for the delayed fit is that upon endothelial injury, PDGF diffuses through the media according to the *full* diffusion–degradation equation $\partial \hat{P}_2/\partial \hat{t} = D_2 \nabla^2 \hat{P}_2 - k\hat{P}_2$: Eqs. (1) and (2) are only good approximations for times $\hat{t} > T$ where T is the time taken for the full problem to (asymptotically) reach its steady state. Hence time points that lie within $[0, T]$ should be ignored as they are not described by Eqs. (1)–(9). What is the value of T? If PDGF degrades very slowly (PDGF may degrade much more slowly than the estimated $k = 0.1$/h in Table 1 when it first binds to proteoglycans in the extra-cellular matrix), then this transient time scale can be estimated from $T = L^2/D_2$ where D_2 is the PDGF diffusivity in the media and L is the media thickness: our assumption is that SMCs start to migrate only when the distribution of PDGF has equilibrated over the *entire* media. There are some wound healing experiments (Nikolic et al., 2006) that suggest that an entire spatially extended population of cells must first be "primed" before they react to chemotactic signals. Hence we take L to be the media thickness since the entire population of SMCs in the media must be "primed" before any migration occurs. With $D_1 = 0.01$ mm^2/h and $L = 1$ mm, we find $T \approx 4$ days, which agrees well with the observation that SMCs only appear in the intima after about 4 days. This delay in migration puzzled the authors in Jackson et al. (1993); our suggested solution is that the period before the onset of SMC migration could be due to a PDGF transient.

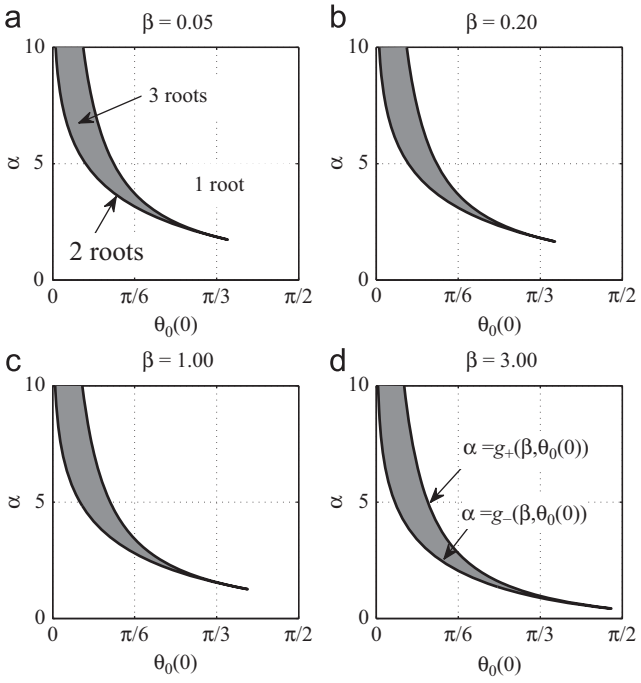

Fig. 7. The number of roots of $F(R)$, as defined in Eq. (23), depends on the value of α, β and $\theta_0(0)$. The boundary between the 3-root and 1-root regions is given by the pair of curves $\alpha = g_{\pm}(\beta, \theta_0(0))$.

In Fig. 8(a) and (b) we fit our model with a fixed value of $\theta_0(0)$. In (b), to maintain a good fit when $\theta_0(0)$ is increased, α and β must decrease. When we allow $\theta_0(0)$ to be determined from least-squares optimization (Fig. 8(c)), we generally find smaller values of α and β and initial angles of injury $\theta_0(0)$ that are close to 2π.

Of the three fitting methods, we find that the delayed fit yields the smallest residual, which supports the transient PDGF hypothesis discussed above. When performing the weighted fit, the value of α is decreased. This is expected since from Eq. (32) we know that $\dot{R}(t = 0)$ is directly proportional to α: when more weight is put on the early points, the slope at $t = 0$ must be smaller and the best-fit value of α must also be smaller. Unfortunately, this method of fitting the data generally results in a larger residual.

By fitting our model to the data, we have derived numerical values for the chemotactic and proliferation parameters α and β. Are these values consistent with the biological and medical literature? Table 2 shows the values of the dimensionless parameters, calculated from Table 1. They are derived from separate experimental and theoretical studies on wound healing, inflammation and atherosclerosis.

If $\theta_0(0)$ is sufficiently large ($\gtrsim \pi/2$), our fitted and calculated values for β are similar, suggesting that the proliferation of SMCs in intimally thickened arteries is comparable to that in cell culture experiments. However fitted values for α in Fig. 8 are much smaller than those from Table 2. Many of the microscopic parameters that define α in Table 1 are taken from studies of PDGF chemotaxis in dermal wound healing assays. Our fitted values are at least 1000× smaller. This suggests that although chemotaxis is common to both wound healing and intimal

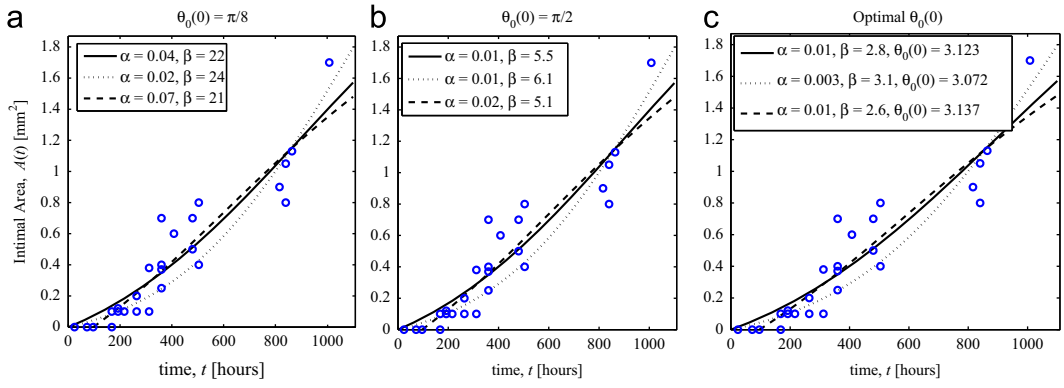

Fig. 8. Comparison of model with data from animal studies (Stadius et al., 1992). For each graph, there are three best-fit curves: solid ("uniform") weights all data points equally, dotted ("weighted") puts 30× more weight on the first four data points and dashed ("delayed") ignores the first four data points. See text for details. The residual for each type of fit is identical across (a), (b) and (c), taking the values 0.61 for the uniform fit, 1.07 for the weighted fit and 0.59 for the delayed fit.

Table 2
Dimensionless parameters for Eq. (23); values are calculated from Table 1.

Symbol	Definition	Approx. value/range
λ_1	$\sqrt{\frac{k}{D_1}}\hat{R}_2$	3
λ_2	$\sqrt{\frac{k}{D_2}}\hat{R}_2$	3
α	$\frac{\rho_s v_0 \chi_0 N_T P_0}{2\rho_0 \hat{R}_2^2 \Pi_1 K_d}$	14–700
β	$\frac{Q_0}{\rho_0 \Pi_1}$	0.06–2
$\theta_0(0)$	–	Variable

thickening, the response in the latter is much weaker. Atherosclerosis is often described as a chronic inflammatory condition. Our analysis supports this description, with SMCs migrating much more slowly and/or in fewer numbers compared to fibroblasts in tissue wounds.

4. Conclusion

In this paper, we presented a model for intimal thickening which is one of the main symptoms of atherosclerosis. The model is a free-boundary problem for the arterial radius; the resulting stenosis is driven by the flux of smooth muscle cells (SMCs) from the media, their proliferation, and death. Migration and proliferation of SMCs in turn is stimulated by platelet-derived growth factor (PDGF) which is released when the endothelium is injured.

The main strength of the model is that it only contains 5 dimensionless parameters: α (migration), β (proliferation), $\theta_0(0)$ (initial angle of injury), λ_1 and λ_2 which are dimensionless diffusivities in the intima and media. Solving the model also allows us to predict how an endothelial injury spreads over time and how PDGF penetrates into different layers of the vessel wall.

We solved our model for a wide range of parameter values. By analyzing the steady states of the equation, we found that a potent mechanism for vessel stenosis was the migration of SMCs from the media leading to further wounding of the endothelium. With the release of more PDGF, the system undergoes positive feedback as more SMCs migrate into the intima. The contraction of the vessel lumen stops abruptly when the entire endothelium is injured ($\theta_0(t)=2\pi$) in which case the stenosed vessel radius saturates at $R\approx\bar{R}=\theta_0(0)/(2\pi)$.

One of the insights that our model provides is that SMC migration is crucial to trigger the onset of intimal expansion in certain systems. Mammals such as mice and rabbits do not normally have pre-existing intimal populations of SMCs. Therefore, for intimal expansion to occur, smooth muscle cells must first migrate from the media; the elaboration of extra-cellular matrix (ECM) and the proliferation of these cells may then cause subsequent enlargement of the intima. On the other hand, humans do have small numbers of SMCs in healthy intima and in principle, these cells could trigger intimal thickening through mitosis.

Our analysis showed that bifurcations can occur in our model giving rise to multiple steady states. The insight generated through our model is that even when the system has reached a stable stenotic state (i.e. migration and proliferation of SMCs is exactly balanced by their death and no further expansion occurs), there are parameter regimes where a small change in cell migration parameters or proliferation rate may give rise to further, sudden stenosis.

Our model makes an important prediction for intimal thickening and eroded plaques: that cell chemotaxis is much weaker than in an acute inflammatory response (e.g. the cell density and/or migration velocity could be much smaller). We arrived this conclusion by fitting our model to data from the stenosed arteries of rabbits and found that the chemotactic parameter α was several orders of magnitude smaller than expected. It should be noted, however, that it was difficult to pin down a precise value for α from the literature. Because there seems to be considerable variability in the pore distribution of the internal elastic lamina, we found a large range of values for the migrating SMC density and therefore a large spread in possible α values.

Although our model is successful in formalizing the main cellular processes that occur in intimal thickening, there are several ways that it can be improved. First, we ignored mechanical stresses in our model by tacitly assuming that remodeling occurs instantly to dissipate residual stress—the governing equation for the luminal radius was derived purely by conserving mass. Second, in Clowes (1983), the authors found that the number of SMCs in the intima rapidly saturated: after two weeks, intimal thickening was caused by accumulation of connective tissue without increase in cell number. Accounting for the elaboration of extra-cellular matrix by intimal SMCs would be a natural extension of our current model. Third, in Jackson et al. (1993), the authors point out from their experiments that platelet depletion inhibits intimal thickening by suppressing migration of SMCs, but it does not stop their replication: there are many other growth factors besides PDGF that are important in intimal thickening. While we assumed the proliferation rate Π_0 to be a function of the local PDGF concentration, it would almost certainly depend on other growth factors as well. Also, although we assumed the death rate Π_1 to be a constant of our equation, there is evidence to suggest that PDGF actually suppresses SMC death (Bennett et al., 1995). Finally, in our model, the angle of injury $\theta_0(t)$ is coupled to the lumen radius $R(t)$ through Eq. (22). This relation is probably too simple; a possible extension would be to separately derive an evolution equation for $\theta_0(t)$ in terms of local endothelial strain and try to describe thrombus growth more explicitly from current models of clot formation (Guy et al., 2007).

Acknowledgements

The author thanks Steve McClure for collecting the data for Fig. 8 and writing a plotting script on MATLAB; Bill Weintraub for useful discussions on atherosclerotic plaque; and the organizers of the Delaware MPI 2009 workshop for introducing the topic of Vulnerable Plaque.

Appendix A. Solution to Helmholtz equation

The solution to (14)–(19) is

$$P_1(r,\theta)=\sum_{m=0}^{\infty}[a_m I_m(\lambda_1 r)+b_m K_m(\lambda_1 r)]\cos m\theta + [c_m I_m(\lambda_1 r)+d_m K_m(\lambda_1 r)]\sin m\theta. \tag{39}$$

$$P_2(r,\theta)=\sum_{m=0}^{\infty}K_m(\lambda_2 r)[A_m \sin m\theta + B_m \cos m\theta], \tag{40}$$

where $I_m(\cdot)$ and $K_m(\cdot)$ are modified Bessel functions of the first and second kind. The constants c_m, d_m, a_m, b_m, A_m and B_m must be determined. Condition (17) implies that

$$\sum_m[a_m I_m(\lambda_1)+b_m K_m(\lambda_1)-B_m K_m(\lambda_2)]\cos m\theta + \sum_m[c_m I_m(\lambda_1)+d_m K_m(\lambda_1)-A_m K_m(\lambda_2)]\sin m\theta=0, \tag{41}$$

or

$$a_m I_m(\lambda_1)+b_m K_m(\lambda_1)-B_m K_m(\lambda_2)=0, \tag{42}$$

$$c_m I_m(\lambda_1)+d_m K_m(\lambda_1)-A_m K_m(\lambda_2)=0. \tag{43}$$

Condition (18) implies that

$$\lambda_2 a_m I_m'(\lambda_1)+\lambda_2 b_m K_m'(\lambda_1)-\lambda_1 B_m K_m'(\lambda_2)=0, \tag{44}$$

$$\lambda_2 c_m I_m'(\lambda_1)+\lambda_2 d_m K_m'(\lambda_1)-\lambda_1 A_m K_m'(\lambda_2)=0. \tag{45}$$

Finally, condition (16) implies that

$$a_m I_m(\lambda_1 R)+b_m K_m(\lambda_1 R)=G_m, \tag{46}$$

$$c_m I_m(\lambda_1 R)+d_m K_m(\lambda_1 R)=H_m, \tag{47}$$

for $m\geq 0$ where

$$G_0=\frac{1}{2\pi}\int_{-\pi}^{\pi} f(\theta)\,\mathrm{d}\theta, \tag{48}$$

$$G_m=\frac{1}{\pi}\int_{-\pi}^{\pi} f(\theta)\cos m\theta\,\mathrm{d}\theta, \quad m>0, \tag{49}$$

$$H_m=\frac{1}{\pi}\int_{-\pi}^{\pi} f(\theta)\sin m\theta\,\mathrm{d}\theta, \quad m\geq 0. \tag{50}$$

Therefore the 6 constants a_m, b_m, c_m, d_m, A_m and B_m are determined by the 6×6 system

$$\begin{bmatrix} I_m(\lambda_1) & K_m(\lambda_1) & 0 & 0 & -K_m(\lambda_2) & 0 \\ 0 & 0 & I_m(\lambda_1) & K_m(\lambda_1) & 0 & -K_m(\lambda_2) \\ I_m(\lambda_1 R) & K_m(\lambda_1 R) & 0 & 0 & 0 & 0 \\ 0 & 0 & I_m(\lambda_1 R) & K_m(\lambda_1 R) & 0 & 0 \\ \lambda_2 I_m'(\lambda_1) & \lambda_2 K_m'(\lambda_1) & 0 & 0 & -\lambda_1 K_m'(\lambda_2) & 0 \\ 0 & 0 & \lambda_2 I_m'(\lambda_1) & \lambda_2 K_m'(\lambda_1) & 0 & -\lambda_1 K_m'(\lambda_2) \end{bmatrix} \begin{bmatrix} a_m \\ b_m \\ c_m \\ d_m \\ B_m \\ A_m \end{bmatrix} = \begin{bmatrix} 0 \\ 0 \\ G_m \\ H_m \\ 0 \\ 0 \end{bmatrix}, \tag{51}$$

so that

$$a_m(R)=[\lambda_1 K_m'(\lambda_2)K_m(\lambda_1)-\lambda_2 K_m(\lambda_2)K_m'(\lambda_1)]G_m(R)/\Delta_m(R), \tag{52}$$

$$b_m(R)=[-\lambda_1 K_m'(\lambda_2)I_m(\lambda_1)+\lambda_2 K_m(\lambda_2)I_m'(\lambda_1)]G_m(R)/\Delta_m(R), \tag{53}$$

$$c_m(R)=[\lambda_1 K_m'(\lambda_2)K_m(\lambda_1)-\lambda_2 K_m(\lambda_2)K_m'(\lambda_1)]H_m/\Delta_m(R), \tag{54}$$

$$d_m(R)=[-\lambda_1 K_m'(\lambda_2)I_m(\lambda_1)+\lambda_2 K_m(\lambda_2)I_m'(\lambda_1)]H_m/\Delta_m(R), \tag{55}$$

$$A_m(R)=[\lambda_2 I_m'(\lambda_1)K_m(\lambda_1)-\lambda_2 I_m(\lambda_1)K_m'(\lambda_1)]H_m/\Delta_m(R), \tag{56}$$

$$B_m(R)=[\lambda_2 I_m'(\lambda_1)K_m(\lambda_1)-\lambda_2 I_m(\lambda_1)K_m'(\lambda_1)]G_m(R)/\Delta_m(R), \tag{57}$$

where

$$\begin{aligned}\Delta_m(R)=&-\lambda_1 K_m'(\lambda_2)[I_m(\lambda_1)K_m(\lambda_1 R)-K_m(\lambda_1)I_m(\lambda_1 R)]\\&+\lambda_2 K_m(\lambda_2)[I_m'(\lambda_1)K_m(\lambda_1 R)-K_m'(\lambda_1)I_m(\lambda_1 R)].\end{aligned} \tag{58}$$

Note that $\Delta_m(R)>0$ if $\lambda_{1,2}>0$ and $0<R<1$. In the special case where

$$f(\theta)=\begin{cases}1, & |\theta|<\min(\theta_0(t)/2,\pi), \quad \theta_0(t)=\theta_0(0)/R\\ 0 & \text{otherwise},\end{cases} \tag{59}$$

we have

$$G_m[R(t)]=\begin{cases}\min\left(\dfrac{\theta_0(0)}{2\pi R(t)},1\right), & m=0,\\ \dfrac{2}{m\pi}\sin\left(\min\left[\dfrac{m\theta_0(0)}{2R(t)},m\pi\right]\right), & m>0,\end{cases} \tag{60}$$

and

$$H_m=0, \quad m\geq 0, \tag{61}$$

so that $c_m=d_m=A_m=0$ for $m\geq 0$ and

$$P_1(r,\theta)=\sum_{m=0}^{\infty}[a_m I_m(\lambda_1 r)+b_m K_m(\lambda_1 r)]\cos m\theta, \tag{62}$$

$$P_2(r,\theta)=\sum_{m=0}^{\infty} B_m K_m(\lambda_2 r)\cos m\theta, \tag{63}$$

For the snapshots in Fig. 3, 50 terms in the above expansions were used.

Appendix B. Estimates of parameters

- *Diffusivities D_1 and D_2*:
  It is difficult to establish definite values for PDGF diffusivities in different regions of the vessel wall from existing literature. However, the transport properties of the intima and media should be different because they have different composition, with the media having a greater density of SMCs. The diffusivity of PDGF in tissue is estimated to be 0.01 mm^2/h in Haugh (2006); this value is lower than the diffusivity in aqueous solution since PDGF is expected to be less mobile in tissues. Also, diffusivities in normal granular and neoplastic tissues (which have an abundance of cancer cells) are compared for different solutes in Chary and Jain (1989) and Gerlowski and Jain (1986). The smaller diffusivity of neoplastic tissues becomes apparent only for large molecular weight substances such as dextran ($\sim$150 kDa) (Gerlowski and Jain, 1986), while the diffusivities of substances such as albumin ($\sim$70 kDa), are very similar (Chary and Jain, 1989). We therefore set up the problem for general $D_1\neq D_2$; however when presenting results, we take $D_1=D_2=0.01$ mm^2/h since PDGF has a molecular weight of about 30 kDa.
- *PDGF concentration P_0*: In Appendix C of Haugh (2006), the author estimates the typical concentration of PDGF in a dermal wound to be 0.1–0.2 nM. Also, in theoretical studies of wound healing (Olsen et al., 1995), typical PDGF concentrations of 10 ng/ml are used. Since PDGF has a molecular weight of $\approx$30 kDa, 10 ng/ml is equivalent to a molar concentration of 0.33 nM which is in rough agreement with Haugh (2006).
- *Pore density of internal elastic lamina ρ_s*: Smooth muscle cells migrate into the intima through pores in the internal elastic lamina (IEL). We can estimate the density of migrating cells by the pore density in the IEL. In Tada and Tarbell (2000), the authors simulate fluid flow through a regular array of circular IEL pores. Two parameters in their IEL model are f, the pore area fraction and d the pore diameter. The distance between two pores is $d\sqrt{\pi/4f}$ from which we estimate the pore density as $4f/\pi d^2$. With f ranging from 0.001 to 0.036 (Tada and Tarbell, 2000) and $d=1$ μm, we find $\rho_s=0.0013$–0.046 μm^{-2}.
- *SMC proliferation rate Q_0*: The proliferation of rat aortic smooth muscle cells *in vitro* under the effects of homocysteine is

studied in Tsai et al. (1994). Data for cell number (per unit area) as a function of time is shown in Fig. 4 of this paper; the proliferation rate Q_0 is estimated from the slope of these curves.

- *SMC death rate*: Π_1 The apoptosis of human vascular smooth muscle cells is studied in Bennett et al. (1995). In these experiments, $8.7 \pm 1.8\%$ or $16.8 \pm 2.7\%$ of the initial SMC population apoptosed within 24 h, depending on the serum used to culture the cells. Assuming exponentially decaying SMC numbers, having 83% to 91% of the initial cell population remaining after 24 h corresponds to k ranging from 4×10^{-3} to 8×10^{-3} h^{-1}. In our study we take the mean value $k = 6 \times 10^{-3}$ h^{-1}. The authors also note that this death rate is much larger than that of normal coronary and aortic vascular SMCs and that PDGF generally suppresses apoptosis of SMCs (in our model, the death rate is independent of PDGF).
- *Chemotactic sensitivity*: χ_0 In chapter 13.4.1 of Keener and Sneyd (2009), the authors present a microscopic model of leukocyte chemotaxis. For rabbit leukocytes responding to the attractant formyl–methionyl–methionyl–methionine (FMMM), they take $\chi_0 = 2 \times 10^5$ cm/receptor.

References

Amar, Martine Ben, Goriely, Alain, Muller, Martin M., Cugliandolo, Leticia. (Eds.), 2011. New Trends in the Physics and Mechanics of Biological Systems: Lecture Notes of the Les Houches Summer School, Volume 92, July 2009. Oxford University Press.

Bennett, M.R., Evan, G.I., Schwartz, S.M., 1995. Apoptosis of human vascular smooth muscle cells derived from normal vessels and coronary atherosclerotic plaques. J. Clin. Invest. 95 (May (5)), 2266–2274.

Bulelzai, M.A.K., Dubbeldam, Johan L.A., 2012. Long time evolution of atherosclerotic plaques. J. Theor. Biol. 297 (March), 1–10.

Calvez, Vincent, Houot, Jean Gabriel, Meunier, Nicolas, Raoult, Annie, Rusnakova, Gabriela, 2010. Mathematical and numerical modeling of early atherosclerotic lesions. ESAIM Proc. 30 (August), 1–15.

Chary, Srikanth R., Jain, Rakesh K., 1989. Direct measurement of interstitial convection and diffusion of albumin in normal and neoplastic tissues by fluorescence photobleaching. Proc. Natl. Acad. Sci. U.S.A. 86 (July), 5385–5389.

Clowes, A.W., 1983. Mechanisms of stenosis after arterial injury. Lab. Invest. 2 (49), 208–215.

Davies, M.J., 1992. Anatomic features in victims of sudden coronary death: coronary artery pathology. Circulation 85, 119–124.

Eftaxiopoulos, Dimitrios A., Atkinson, Colin, 2005. A nonlinear anisotropic and axisymmetric model for balloon angioplasty. Proc. R. Soc. A Math. Phys. Eng. Sci. 461 (March (2056)), 1097–1128.

Farb, Andrew, Burke, Allen P., Tang, Anita L., Liang, Youhui, Mannan, Poonam, Smialek, John, Virmani, Renu, 1996. Coronary plaque erosion without rupture into a lipid core: a frequent cause of coronary thrombosis in sudden coronary death. Circulation 93 (7), 1354–1363.

Fok, Pak-Wing, 2011. Growth of necrotic cores in atherosclerotic plaque. Math. Med. Biol. in press, http://dx.doi.org/10.1093/imammb/dqr012.

Gerlowski, L.E., Jain, R.K., 1986. Microvascular permeability of normal and neoplastic tissues. Microvasc. Res. 305, 288–305.

Goriely, A., Vandiver, R., 2010. On the mechanical stability of growing arteries. IMA J. Appl. Math. 75 (April (4)), 549–570.

Guy, Robert D., Fogelson, Aaron L., Keener, James P., 2007. Fibrin gel formation in a shear flow. Math. Med. Biol. J. IMA 24 (March (1)), 111–130.

Haugh, Jason M., 2006. Deterministic model of dermal wound invasion incorporating receptor-mediated signal transduction and spatial gradient sensing. Biophys. J. 90 (7), 2297–2308.

Ibragimov, A.I., McNeal, C.J., Ritter, L.R., Walton, J.R., 2005. A mathematical model of atherogenesis as an inflammatory response. Math. Med. Biol. J. IMA 22 (December (4)), 305–333.

Jackson, C.L., Raines, E.W., Ross, R., Reidy, M.A., 1993. Role of endogenous platelet-derived growth factor in arterial smooth muscle cell migration after balloon catheter injury. Arteriosclerosis Thromb. Vasc. Biol. 13, 1218–1226.

Keaney, J.F. (Ed.), 2000. Oxidative Stress and Vascular Disease. Kluwer Academic Publishers.

Keener, J., Sneyd, J., 2009. Mathematical Physiology II: Systems Physiology. Springer.

Kolodgie, F.D., Burke, A.P., Farb, A., Weber, D.K., Kutys, R., Wight, T.N., Virmani, R., 2002. Differential accumulation of proteoglycans and hyaluronan in culprit lesions: insights into plaque erosion. Arteriosclerosis Thromb. Vasc. Biol. 22, 1642–1648.

Newby, A.C., Zaltsman, A.B., 1999. Fibrous cap formation or destruction—the critical importance of vascular smooth muscle cell proliferation, migration and matrix formation. Cardiovasc. Res. 41 (February (2)), 345–360.

Nikolic, D.L., Boettiger, A.N., Bar-Sagi, D., Carbeck, J.D., Shvartsman, S.Y., 2006. Role of boundary conditions in an experimental model of epithelial wound healing. Am. J. Physiol. Cell Physiol. 291, 68–75.

Olsen, Luke, Sherratt, Jonathan A., Maini, Philip K., 1995. A mechanochemical model for adult dermal wound contraction and the permanence of the contracted tissue displacement profile. J. Theor. Biol. 177 (2), 113–128.

Ougrinovskaia, Anna, Thompson, Rosemary S., Myerscough, Mary R., May 2010. An ODE model of early stages of atherosclerosis: mechanisms of the inflammatory response. Bull. Math. Biol. 1534–1561.

Park, Chang Shin, Schneider, Ian C., Haugh, Jason M., 2003. Kinetic analysis of platelet-derived growth factor receptor/phosphoinositide 3-kinase/Akt signaling in fibroblasts. J. Biol. Chem. 278 (September (39)), 37064–37072.

Roger, Véronique L., Go, Alan S., Lloyd-Jones, Donald M., Benjamin, Emelia J., Berry, Jarett D., Borden, William B., Bravata, Dawn M., Dai, Shifan, Ford, Earl S., Fox, Caroline S., Fullerton, Heather J., Gillespie, Cathleen, Hailpern, Susan M., Heit, John A., Howard, Virginia J., Kissela, Brett M., Kittner, Steven J., Lackland, Daniel T., Lichtman, Judith H., Lisabeth, Lynda D., Makuc, Diane M., Marcus, Gregory M., Marelli, Ariane, Matchar, David B., Moy, Claudia S., Mozaffarian, Dariush, Mussolino, Michael E., Nichol, Graham, Paynter, Nina P., Soliman, Elsayed Z., Sorlie, Paul D., Sotoodehnia, Nona, Turan, Tanya N., Virani, Salim S., Wong, Nathan D., Woo, Daniel, Turner, Melanie B., 2012. Heart disease and stroke statistics—2012 update: a report from the American Heart Association. Circulation 125 (January (1)), e2–e220.

Schneider, Ian C., Haugh, Jason M., 2005. Quantitative elucidation of a distinct spatial gradient–sensing mechanism in fibroblasts. J. Cell Biol. 171 (December (5)), 883–892.

Shaw, L.A., Rudin, M., Cook, N.S., 1995. Pharmacological inhibition of restenosis: learning from experience. Trends Pharmacol. Sci. 16 (December (12)), 401–404.

Stadius, M.L., Rowan, R., Fleischhauer, J.F., Kernoff, R., Billingham, M., Gown, A.M., 1992. Time course and cellular characteristics of the iliac artery response to acute balloon injury. An angiographic, morphometric, and immunocytochemical analysis in the cholesterol-fed New Zealand white rabbit. Arteriosclerosis Thromb. Vasc. Biol. 12, 1267–1273.

Tada, S., Tarbell, J.M., 2000. Interstitial flow through the internal elastic lamina affects shear stress on arterial smooth muscle cells. Am. J. Physiol. Heart Circ. Physiol. 278, H1589–H1597.

Thubrikar, M., 2007. Vascular Mechanics and Pathology. Springer.

Tsai, J.-C., Perrella, M.A., Yoshizumi, M., Hsieh, C.-M., Haber, E., Schlegel, R., Lee, M.-E., 1994. Promotion of vascular smooth muscle cell growth by homocysteine: a link to atherosclerosis. Proc. Natl. Acad. Sci. U.S.A. 91, 6369–6373.

Vincent, P.E., Plata, A.M., Hunt, A.A.E., Weinberg, P.D., Sherwin, S.J., 2011. Blood flow in the rabbit aortic arch and descending thoracic aorta. J. R. Soc. Interface, 1708–1719.

Virmani, R., Narula, J., Leon, M.B., Willerson, J.T. (Eds.), 2007. The Vulnerable Atherosclerotic Plaque. Blackwell Futura.